



Agent-based epidemiological modeling of COVID-19 in localized environments[☆]

P. Ciunkiewicz^{a,*}, W. Brooke^b, M. Rogers^b, S. Yanushkevich^c

^a Department of Biomedical Engineering, University of Calgary, Calgary, AB, Canada

^b Schulich School of Engineering, University of Calgary, Calgary, AB, Canada

^c Department of Electrical and Computer Engineering, University of Calgary, Calgary, AB, Canada



ARTICLE INFO

Keywords:

Agent-based simulation
Decision support
Machine reasoning
Risk
Epidemiological model
COVID-19

ABSTRACT

Epidemiological modeling is used, under certain assumptions, to represent the spread of a disease within a population. Information generated by these models can then be applied to inform public health practices and mitigate risk. To provide useful and actionable preparedness information to administrators and policy makers, epidemiological models must be formulated to model highly localized environments such as office buildings, campuses, or long-term care facilities. In this paper, a highly configurable agent-based simulation (ABS) framework designed for localized environments is proposed. This ABS provides information about risk and the effects of both pharmacological and non-pharmacological interventions, as well as detailed control over the rapidly evolving epidemiological characteristics of COVID-19. Simulation results can inform decisions made by facility administrators and be used as inputs for a complementary decision support system. The application of our ABS to our research lab environment as a proof of concept demonstrates the configurability and insights achievable with this form of modeling, with future work focused on extensibility and integration with decision support.

1. Introduction

The virus SARS-CoV-2 was first discovered in December 2019, in Wuhan, China. It is a novel coronavirus that causes the disease known as COVID-19. SARS-CoV-2 quickly spread around the world, causing the World Health Organization to declare a COVID-19 pandemic on March 12, 2020 [1]. As of August 11, 2021, there have been 204,944,144 cases and 4,312,902 deaths linked to the disease [2]. Multiple waves of COVID-19 have occurred and it has been shown that non-pharmacological interventions (NPIs) such as masking and physical distancing, as well as pharmacological interventions such as vaccines, help mitigate disease spread [3–7].

Agent-based models consist of a group of individual entities known as agents, whose behaviour and decision-making is based on simple rules [8,9]. Even with simple guiding rules, these simulations can reveal emergent or unexpected properties in their modeled environments [10–17]. This paper develops an agent-based simulation (ABS)

framework to examine the spread of COVID-19 and applies it within a university research lab environment.

Contemporary epidemiological models (EMs) provide information about the risk related to a disease spreading, based on evidence from past epidemics or pandemics. In the early stages of an epidemic when limited data is available, mathematical forecasting tools such as compartmental models are used, with stochastic models introducing variation. Many assumptions are required for both compartmental and stochastic modeling, limiting their reliability to the strength of the assumptions. Fractional mathematical models have also been applied at a population level due to their nonlocal character, overcoming certain limitations of other models [18–20]. Increasingly complicated agent-based models can be used to more accurately describe population behaviour and movements as additional data becomes available [21]. All of these models can predict parameters such as attack rate, case fatality rate, or infection prevalence rate (IPR), but they are often applied on a large population-scale and do not necessarily account for the

[☆] This document is the results of the research project funded by the Brenda Strafford Foundation; Alberta Innovates; and the Natural Sciences and Engineering Research Council of Canada. The former is a non-profit organization that provides grants and scholarships to the University of Calgary and the latter is a provincial government award.

* Corresponding author.

E-mail address: philip.ciunkiewicz@ucalgary.ca (P. Ciunkiewicz).

uncertainties of individual behaviour. Modeling results are generally contextualized by attack rate: the proportion of a susceptible population that contracts a disease over an outbreak period, and case fatality rate: the proportion of a population that dies due to having contracted the disease [22].

It is necessary to develop an agent-based model that can be applied to smaller, highly localized, and variable environments. Such a model would also account for realistic individual behaviour. This paper proposes such a model and offers the example of our research lab to demonstrate that disease spread and individual behaviour can be modeled accurately to provide actionable insights to administrators who are not experts in the field of epidemiology.

Subsequent sections of this paper are structured as follows. Section 3 describes the methodology, construction, and operation of the ABS, along with experimental configuration for the proof of concept. Section 4 details the simulation outputs and select extracted insights. Section 5 discusses the benefits of providing a highly configurable ABS for modeling disease spread. Section 6 concludes our findings as well as providing multiple promising avenues for future exploration and development.

2. Objectives and contributions

This research seeks to accomplish the following:

- Develop a simulation framework to forecast COVID-19 transmission in localized environments, accounting for epidemiological parameters, airborne viral spread, vaccination, and masking.
- Provide useful data that can be converted to the epidemiological concepts of attack rate, case fatality rate, and risk.
- Present these epidemiological results to facility administrators in an interpretable and actionable manner.

Facility administrators are not necessarily experts in the field of epidemiological preparedness, and the proposed ABS provides clear information about risks and how they can be mitigated with different interventions. This paper contributes to the modeling of disease spread for epidemiological preparedness. The key contribution is threefold:

1. Development of an ABS, with a focus on the effects of policy and preventative action.
2. Offering a decision support system for non-experts in facility administration, allowing for a more rapid educated response to future disease outbreaks.
3. Reducing risk and negative epidemiological outcomes associated with inaction or improper reaction.

3. Methods

This paper proposes an ABS similar to Ref. [15], which uses an agent-based EM to simulate the spread of COVID-19 within an elderly care facility. It considers staff and resident behaviour (including contact patterns), the age-dependent risk of severe outcomes (hospitalization or death), and epidemiological parameters such as the length of the incubation and infectious periods. In Refs. [23–25], the authors examine COVID-19 transmission on a smaller scale, using computational fluid dynamics to model aerosol transport caused by exhalation and coughing. Those principals are simplified and combined for this paper to be applied in a generalizable way using diffusion to model viral particle spread.

The ABS is designed to be highly modular using an object-oriented-programming approach. The proposed software structure allows for very rapid generalization to different diseases, scenarios, and environments with minimal software development required. Ease of use and integration with new facilities will reduce the overhead of implementation for such a system, increasing the likelihood of adoption by

various facilities. The ABS proposed in this paper is defined by the following informational class hierarchy:

- Agents
 - Represent the base informational unit,
 - Interact within the simulation.
- Simulation Scenario
 - Contains all of the agents,
 - Contains information from Fig. 1a.
- Simulation Model
 - Organizational tool for executing agent behaviour,
 - Orchestrating evolution within a specific scenario.

The proposed ABS is designed to be configured for use in any localized scenario. Important configurable parameters are defined in Fig. 1a. The basic input data required for the ABS is illustrated in Fig. 1b.

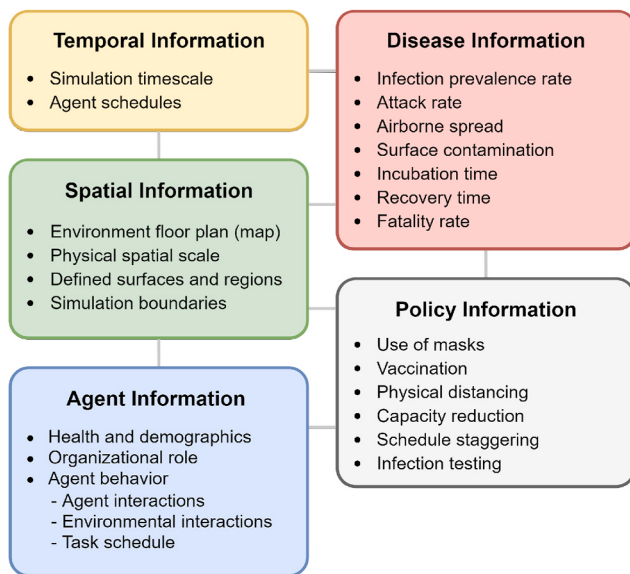
3.1. Agents

All agents in the model belong to the base agent class. The base agent class contains information about the agent's location, subclass, schedule, epidemiological status, and "prevention index". The location of the agent, stored as a Cartesian coordinate triplet (x, y, z), tracks their spatial position with respect to other agents and the environment (scenario map) itself. An agent's subclass reflects the role they have within the model and determines their behavior, scheduling, and which areas within the scenario map they have access to. Individual agent schedules further determine where and when the agent travels within the scenario map in more detail. The agent's epidemiological status also informs their behaviour and contains information relating to their health. Each agent additionally has a "prevention index", which describes how they are protected from infection by vaccination and masking.

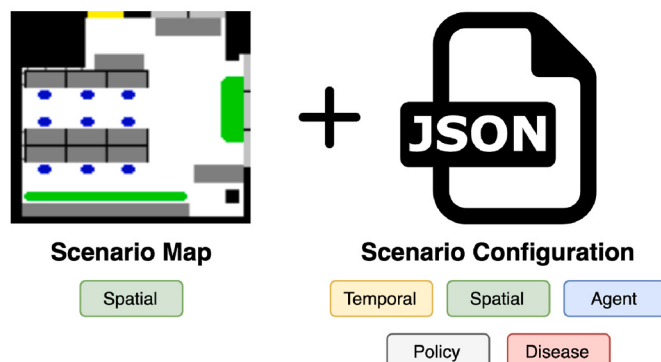
Agent subclasses are based on roles reflecting real-world facilities. Using long-term care facilities (LTCFs) as an example: subclasses could include "healthcare worker", "non-healthcare worker", "resident", and "visitor". An agent's subclass directly affects their schedule and which regions of the scenario map an agent is able to access. For example, if an agent belongs to the "resident" subclass, their schedule might include staying in their room or accessing communal spaces. Such an agent would not be able to access administrative stations. Conversely, agents belonging to the "healthcare worker" subclass would be more mobile as they move between multiple rooms in the scenario map to simulate interaction with residents. These agents would also be able to access certain areas such as administrative stations and staff-only rooms which other subclasses cannot. Schedule characteristics for agents of different subclasses are determined through consultation with facility administration. Day-to-day variance in an agent's schedule occurs by stochastically sending agents earlier or later to their objectives.

The epidemiological status of an agent is assigned according to Fig. 2. Having a particular status effects agent behaviour as well as future risk of infection. For example, an agent with the status of QUARANTINED will remove themselves from the simulation for the required time period, while it is assumed that an agent with the RECOVERED status cannot be as readily reinfected with the disease. Additionally, the instant an agent is infected, the simulation has knowledge of it. If the agent is presymptomatic or remains asymptomatic for the duration of the infection (subject to probabilities based on epidemiological parameters), the agent will not quarantine. Because the simulation has knowledge of the infection, such an agent will continue on their regular schedule and possibly infect other agents.

Each agent is also assigned a "prevention index," which describes how their risk of becoming infected decreases with vaccines and masking. A "prevention index" of 0.0 means the agent has no form of protection against infection, while a "prevention index" of 1.0 means the agent is completely protected. Each agent's "prevention index" is different and is constructed from the type of vaccine, dosage level, and



(a) Configurable parameters for the simulation. Each labeled group of parameters is independently configurable, however certain parameters are closely related and influence each other (such as temporal and agent information for scheduling).



(b) Basic input data required for the simulation. The scenario map includes one or more RGB images of the environment floor plan, to scale. Pixel color values delineate different terrain types, such as desks, chairs, the exit, etc. The scenario configuration is a series of JSON objects detailing the full set of configurable parameters for the simulation, including an explicit reference to the scenario map file(s).

Fig. 1. Simulation configuration and inputs.

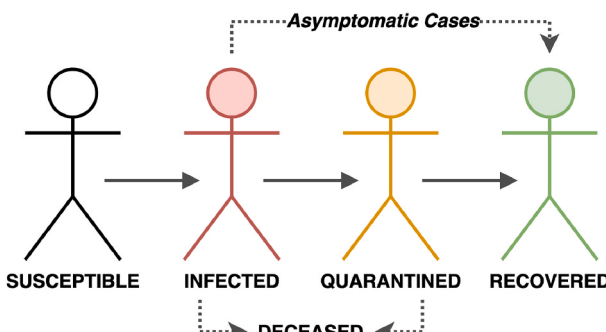


Fig. 2. Possible epidemiological statuses for agents. Solid arrows represent typical disease progression, dotted arrows represent rare cases.

type of mask, based on reported efficacy in the literature [3–7]. The corresponding values for each prevention method are described in Table 1.

3.2. Infection portrait

The infection portrait defines all parameters related to the infection that is being monitored, which in the case of the proposed ABS is COVID-19. This includes: considered methods of transmission; the number of initial infections; parameterizing how viral particles are released by breathing agents and spread through the environment; and information about disease progression once an agent is infected such as the length of the presymptomatic (incubation) and recovery periods, percentage of cases that remain asymptomatic, etc.

In the proposed ABS, both droplet and aerosol transmission are considered. Droplet transmission occurs primarily when agents are close together (within 1 m). If one of the agents is infected, the droplets they produce when breathing, speaking, and coughing can be ingested through the mouth or nose, causing infection [26].

Aerosol transmission of COVID-19 occurs when small particles (smaller than those considered in droplet transmission) are released into the air by infected agents through breathing and speaking [27]. These aerosol particles are small enough to remain in the air for hours, and can travel much farther than droplets [28]. As the infected agent exhales, the aerosol particles they generate begin to diffuse into the environment, spreading outwards radially and lingering in the air. Susceptible agents inhaling these aerosol particles are at risk of infection [23].

Other research has focused on viral spread through fomite transmission in similar environments, including the spread of norovirus by the fecal-oral route. While research on SARS-CoV-2 has suggested that it may spread by fomite transmission, we are currently considering this to be outside the scope of this proof of concept.

The number of infected agents initially present in the model is variable. At the start of each “run” of the simulation, each agent has a 0.021 probability of being infected, based on Canada’s test positivity rate (7 day moving average) at the time of this writing [29]. This value of 0.021 will be used as the IPR in simulation runs for the proof of concept proposed in this study.

The length of the presymptomatic and recovery periods are both sampled from log-normal distributions [12,24]. The log-normal distribution for a variable X is given by

$$X = e^{\mu + \sigma Z} \quad (1)$$

where Z is a standard normal variable, and μ, σ are the respective mean and standard deviation of the natural logarithm of X instead of X itself. As a probability density function, $f_X(x)$ is rewritten as

$$f_X(x) = \frac{1}{x\sigma\sqrt{2\pi}} \exp\left(-\frac{(\ln x - \mu)^2}{2\sigma^2}\right). \quad (2)$$

A different log-normal distribution is used for the cases that display severe symptoms, representing 16% of cases [12]. Additionally, 17% of cases remain asymptomatic for the duration of the infection and the agent does not display symptoms while spreading the virus [30].

Table 1

Prevention index values for masking and vaccination based on reported efficacy in preventing virus transmission. No mask and no vaccination have corresponding prevention index values of zero.

Mask	Vaccine	
	1 Dose	2 Dose
Cloth 0.3	Surgical 0.5	N95 0.85
		Any 0.31
		AstraZeneca 0.67
		Pfizer/Moderna 0.88

3.3. Disease life cycle modeling

The initial version of the ABS is based on the Susceptible-Infected-Recovered (SIR) model [31]. It considers each agent belonging to one of the following states: Susceptible, Infected, or Recovered. Such models are common in epidemiology to simulate disease spread. The SIR model is governed by differential equations provided by eq. (3) [31].

$$\frac{dS}{dt} = -\frac{\beta IS}{N}; \quad \frac{dI}{dt} = \frac{\beta IS}{N} - \gamma I; \quad \frac{dR}{dt} = \gamma I. \quad (3)$$

Here S , I , and R denote the susceptible, infected, and recovered populations respectively, while N represents the total population. Each β and γ are epidemiological parameters representing infection and recovery characteristics respectively, with the ratio $R_0 = \beta/\gamma$ defining the basic reproduction number.

While these state models are usually applied at a population level with differential equations describing population flow between states, we are using an SIR model to inform how diseases progress in a highly localized environment. For the purposes of our model, we are considering the “R” state as “removed” rather than “recovered”. The “removed” state includes agents who either recovered from the disease or are deceased. This means that agents with epidemiological statuses of either RECOVERED or DECEASED are considered to be “removed” from the perspective of the SIR model.

3.3.1. Agent perspective - SI(q)R model

As applied to an individual, the core of the SIR model can be represented as a finite state machine. The state transition from SUSCEPTIBLE to INFECTED is determined by the disease spread model. For our implementation, the recovery period is the length of time it takes an agent to recover from COVID-19, transitioning from INFECTED to RECOVERED.

As agent-based models are most useful for observing the effects of individual behavior, an additional QUARANTINED state was added to the basic SIR model. This state has no impact on disease progression or contagion, but does change agent behavior. Within the model, this is denoted by an agent having an epidemiological status of QUARANTINED. It is assumed that an agent displaying signs or symptoms of COVID-19 will self-isolate for 14 days based on public health guidelines [32]. Infected agents will display signs or symptoms at different times, based on the length of the presymptomatic period while some remain asymptomatic [30].

3.3.2. Disease perspective - SIR model with airborne spread

The ABS maintains data on the level of viral particles in the air for the same discretized space-time underlying agent behavior, illustrated in Figs. 3 and 4. As with agent behaviour, the viral level is determined according to a simple set of rules. These rules are applied once per each simulation time-step.

- Susceptible agents in a location with non-zero viral level have a chance of becoming infected. This chance is linearly scaled by the viral level, adhering to the independent action hypothesis.
- Infectious agents shed virus, increasing the viral level in their location.
- Viral level in a location exponentially decays over time.
- Virus particles diffuse radially outward from an infectious agent

The application of these rules results in a disease spread that matches current public health messaging about COVID-19: most infection occurs when a susceptible individual is experiencing close sustained contact with an infected individual. From the SIR model perspective, the simulation effectively treats the additional QUARANTINED state as the INFECTED state with instructions to vacate the environment. Fig. 3 illustrates the basic operation of the simulation at a high level. Fig. 4

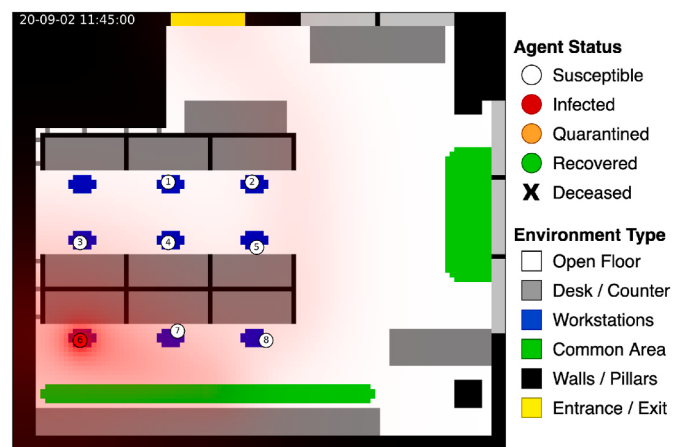


Fig. 3. Example frame visualization from the scenario simulation. Viral particle concentration is shown as a transparent red overlay. Agents numbered 1–8 (ascending left-to-right, top-to-bottom) are seated as they would be in our lab environment. (For interpretation of the references to color in this figure legend, the reader is referred to the Web version of this article.)

shows the movement of an agent through space and time, as well as the progression of viral concentration and various other parameters.

3.4. Agent behavior

An ABS requires well-defined agent behavior to achieve meaningful results, which in this proof of concept is designed to mimic the behaviour of researchers in our lab. Implementing a system in which agents adhere to a schedule relies on three fundamental pieces of technical infrastructure: positional awareness, temporal awareness, and ability to execute tasks.

3.4.1. Positional awareness

Positional awareness in the context of simulated agents has two components: individual agent position within the environment, and environmental elements such as walls, doors, restricted areas, etc. The agent's own position is important for most of the computations performed at each discrete time-step in the simulation. These computations include both environmental interactions such as the disease spread mechanics and behavioral mechanics such as taking the optimized path to a specific location. The scenario map includes various terrain types, such as communal spaces, private rooms, and administrative stations. Some terrain is off-limits to all agents, including walls and other non-walkable areas.

3.4.2. Temporal awareness

Agents must have temporal awareness to track movement in time, including current position, target position, and relative position of other agents at the same point in time. Scheduling the behavior of agents relies on all agents operating on the same universal time, and the same is true for simulating the disease spread mechanics. This universal time is achieved by simulating all agents over global discrete time-steps which are associated with the underlying scenario. Data gathered during the run-time of the simulation is tracked with respect to these global time-steps, with temporal resolution configurable at the scenario level.

3.4.3. Task execution

Task execution utilizes the basic infrastructure established by positional and temporal awareness to add dynamic behavior to the agents. A task in this context can be abstracted as an instruction to move an agent to a specified location and stay at that location for a specified duration of time. Of course, these tasks represent the objectives that different people in a real-life LTCF would carry out each day. Each task assigned to an

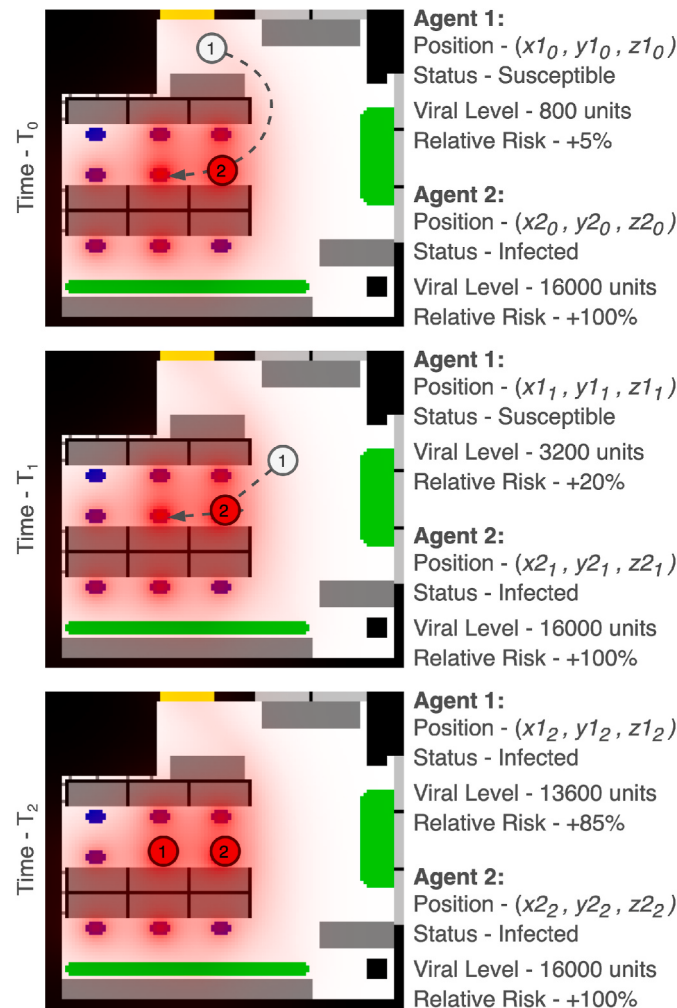


Fig. 4. Evolution of agent and scenario parameters over time in the simulation. The spatial position of Agent i at time-step j is given as the Cartesian coordinate triplet (x_{ij}, y_{ij}, z_{ij}) . Viral level and corresponding relative risk are reported on a unitless scale with a ceiling of 16,000 units at the direct location of an infected agent, representing +100% relative risk. Each vertical frame represents a time-step, with an explicit arrow showing the path of the agent through the environment. As the susceptible agent 1 moves to areas with higher airborne viral concentrations (denoted by transparent red image layer) near infected agent 2, their relative risk of infection per unit time increases. Once the agent becomes infected through probabilistic transmission mechanisms based on reported proximity and co-occupancy time in the literature, they begin spreading viral particles and further increasing the local viral level through spatial diffusion. (For interpretation of the references to color in this figure legend, the reader is referred to the Web version of this article.)

agent requires transit from the current position, A , to a target position, B . Operating under the assumption that agents will opt to take the fastest route connecting points A and B , the shortest direct path between these points must be computed. Each agent also progresses to each objective based on a level of “urgency” that describes how quickly they will move through the environment.

Many algorithms exist for optimizing paths, however for the purposes of this simulation the best option was found to be the A* (A-star) algorithm. This algorithm was developed in the 1960s for solving problems in robotics, and it was primarily chosen due to the relative performance scaling when compared to other search algorithms [33,34]. The algorithm selects a path which iteratively minimizes the cost function f defined in eq. (4).

$$f(n) = g(n) + h(n) \quad (4)$$

Here n represents the next possible move along the path. Term $g(n)$ denotes the “current” cost of the path between initial point n_i and n , and $h(n)$ is a heuristic function estimating the lowest cost path between n and final point n_f .

The specific implementation used allows for the environment to be represented as a 2D matrix, with elements representing discrete spatial regions of the environment and directly adjacent elements (cardinal and diagonal) representing possible moves by the agent. Elements are assigned weights based on the respective terrain type, representing the associated cost of traversal in the cost function. Non-walkable terrain such as walls or furniture are masked with zero-values to infinitely increase the cost of a solution which paths the agent through them. If the weight of a non-zero element is set sufficiently high (greater than the sum of all regularly weighted elements), the agent will attempt to traverse all other regions in the environment before returning to the non-walkable terrain.

3.4.4. Defining behavioral patterns

The base agent class is defined only with the fundamental infrastructure required for task execution. This modular approach supports defining behavioral patterns independently of base agent function, allowing the simulation to support a diverse range of agent archetypes. Task execution is related closely to an agent’s schedule, which is dependent on its subclass.

Using the environment of a LTCF as an example, there are multiple types of agents with different behavior and schedules that must be simulated: healthcare workers adhere to strict schedules and are free to move between different areas throughout the day, and during the night some will leave the facility and some will stay; non-healthcare workers have scheduled tasks during the day at set locations in the facility and may have limited access to some areas, leaving the facility at night; residents may move freely between their rooms and communal spaces, but will also follow a set schedule, returning to their rooms at night. This approach can be applied to any environment, simulating complex disease spread realistically with basic and scalable agent behavior.

3.5. Simulation configuration and experimental setup

For this proof of concept, the experimental setup is as follows. Our research lab environment is used as a basis for simulating all scenarios. Agents are directly modeling the behavior and schedules of researchers in the lab across ~ 210 h of contact (5-s simulated temporal resolution for 150,000 time-steps). A sample daily schedule for an agent researcher in the lab is provided in Table 2. The environment is only simulated between 7am and 7pm while agents are present, with full disinfection occurring between days. The following epidemiological scenarios are explored and reported in this proof of concept:

- Masking:

- No masking (“nomask”),
- Cloth masks (“cloth”),
- Surgical masks (“surgical”),
- N95 respirators (“n95”).

Table 2

Sample daily schedules for select agent researchers in the simulated lab environment.

Times	Agent 1	Times	Agent 2	Times	Agent 3
07:40	WORK	09:00	WORK	09:00	WORK
07:45	TEA	12:00	EXIT	09:20	TEA
09:10	TEA	14:00	WORK	12:00	TEA
11:00	EXIT	15:40	TEA	13:00	EXIT
11:20	WORK	16:30	EXIT	13:40	WORK
11:30	TEA			18:30	EXIT
17:00	EXIT				

- Vaccination:
 - No vaccination (“novax”),
 - One dose any vaccine (“1dose”),
 - Two doses Oxford AstraZeneca (“astr”),
 - Two doses Pfizer/Moderna mRNA (“mrna”).
- Physical distancing: normal desk spacing.
- Capacity reduction: eight actors total.
- Schedule staggering: normal observed schedules.
- Infection testing: none applied.

The combination of each masking and vaccination option provides 16 unique scenarios to explore for this proof of concept. An example of one scenario is the combination “surgical” + “novax”. In this scenario all agents adhere to surgical mask requirements and are unvaccinated. Each unique scenario is simulated for 10,000 ensemble trials to provide sufficient data for analysis. The simulation outputs the following raw data per time-step:

- Virus matrix (shape of environment map)
 - Per-pixel viral concentration in space
- Agent information
 - Spatial location (x, y, z)
 - SI(q)R epidemiological status
- Temporal index (date-time timestamps)

4. Results

Results generated by this proof of concept model are focused on the 16 possible mask and vaccine combinations defined, with policy effectiveness based on external studies exploring pharmacological and non-pharmacological interventions (summarized in Table 1) [3–7]. Analysis of the raw results explored in this paper includes only a subset of possible investigations. For analyses which are not comparing multiple scenarios, the nomask-novax combination is used.

4.1. Non-comparative analysis

Fig. 5 illustrates the epidemic trajectory curves as both a cumulative stackplot (top) and line chart (bottom). For the nomask-novax scenario, the peak of infections (INFECTED + QUARANTINED) occurs between 60 and 72 h of exposure, representing between five and six 12-h workdays. After 210 h of exposure the number of infections has nearly plateaued out with a final recovered proportion of 0.038.

Fig. 6 plots the average excess risk of infection beyond the population IPR per agent as a time series. Agent numbering reflects the seating structure shown in **Fig. 3** and respective behavior based on observed daily schedules. For the nomask-novax scenario, individual agents experience significantly different excess risk, ranging from 0.010 to 0.022 after 210 h of exposure. Observing lines of constant-risk (i.e. constant y) will demonstrate how much time exposure will incur similar risk for an agent. For example at $y = 0.010$, agent 1 intersects at $x = 60$ h while agent 6 intersects at $x = 210$ h, representing a tripling in exposure time to incur the same level of risk. Conversely observing lines of constant-time (i.e. constant x) will demonstrate the incurred risk at the same level of exposure. There are two apparent clusters which emerge after 75 h of exposure: agents 3, 6, 8; and agents 1, 2, 4, 5, 7.

4.2. Comparative analysis

Fig. 7 shows the average excess risk of infection across all agents for different scenarios. In all comparisons, a higher prevention index results in a reduced excess risk of infection. The magnitude of this reduction is proportional to the magnitude of the compound prevention index. As with **Fig. 6**, lines of constant-risk (i.e. constant y) illustrate time taken to incur set risk, and lines of constant-time illustrate risk incurred at the exposure level. For example in **Fig. 7** at $x = 125$ h, agents with n95 masks

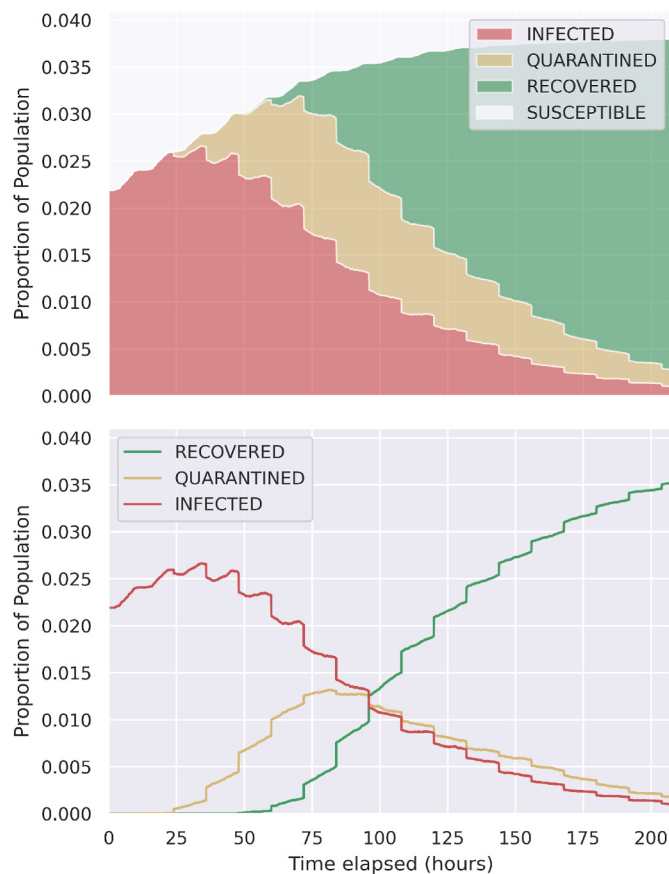


Fig. 5. Average infection and recovery numbers over time from 10,000 scenario simulations as a stackplot (top) and line chart (bottom). Scenario simulated for no-mask, no-vaccine, and an infection prevalence rate of 0.021.

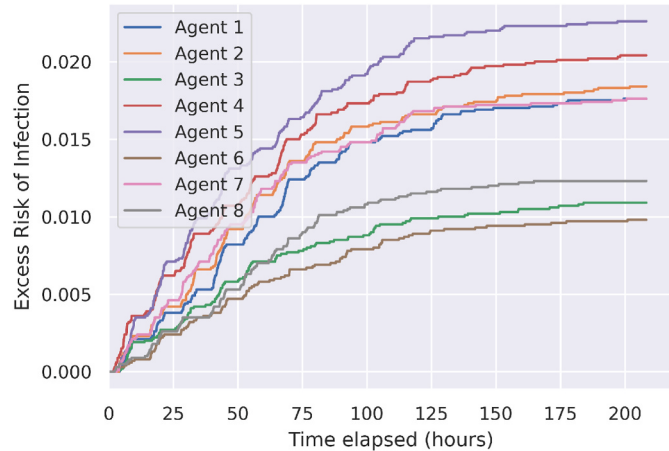


Fig. 6. Average excess risk (probability of infection) experienced by agents over time from 10,000 scenario simulations. Scenario simulated for no-mask, no-vaccine, and an infection prevalence rate of 0.021.

experience 10% excess risk while agents with surgical masks experience 33% excess risk, representing a 330% increased level of risk at the same exposure time. Similarly, at $x = 125$ h agents with 1-dose of vaccine experience a 500% increase in excess risk over agents with 2-dose mRNA vaccine.

Fig. 8 illustrates the final excess risk of infection per agent for all 16 scenarios combining masking and vaccination measures. As with **Fig. 6**, agent numbering reflects the seating structure shown in **Fig. 3** and

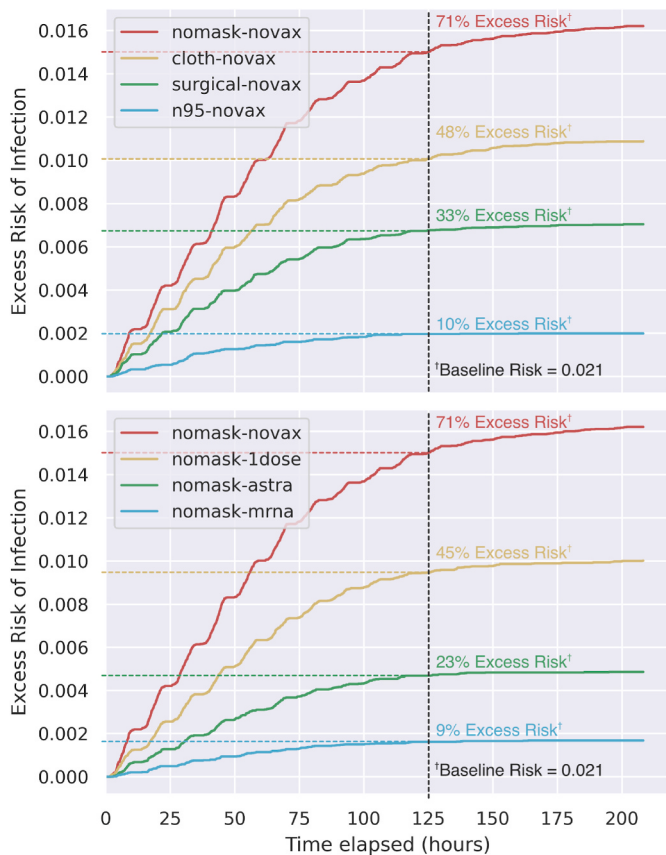


Fig. 7. Effect of masking (top) and vaccination (bottom) on average excess risk (probability of infection) experienced by agents over time from 10,000 scenario simulations. Scenario simulated for an infection prevalence rate of 0.021. Percent excess risk is calculated from this baseline value of 0.021.

respective behavior based on observed daily schedules. It can be seen that there are clear trends between agents based on the compound prevention index, and similarly there are clear trends between scenarios based on the specific agent being studied. The highest excess risk is marked as red and associated with the nomask-novax scenario, while the lowest excess risk is marked as green and associated with the n95-mrna scenario. The color map is logarithmically scaled to better capture the range of excess risk. An excess risk of 10^{-2} represents a ~50% increase over the population IPR of 0.021, while an excess risk of 10^{-4} represents a ~0.5% increase. Agents 3, 6, and 8 consistently have lower excess risk than the others, while agents 2, 4, and 5 consistently have higher excess risk.

5. Discussion

In this study we proposed a highly configurable agent-based approach to modeling disease spread in localized environments. Focusing specifically on modeling localized environments provides a distinct benefit over large-scale and equation-based EMs by offering decision support insights at a granular level. Different environments and facilities have unique challenges in epidemic management based on numerous factors, including architectural characteristics, population and demographic distribution, and specific risk tolerance. These challenges are often not taken into account when using large-scale or equation-based EMs, resulting in policy decisions which may not be appropriate for all environments. Conversely, existing localized agent-based modeling techniques are highly specific, targeting limited environments without strong emphasis on configurability [10,13,15,23]. This focused scope results in limited utility provided by these models

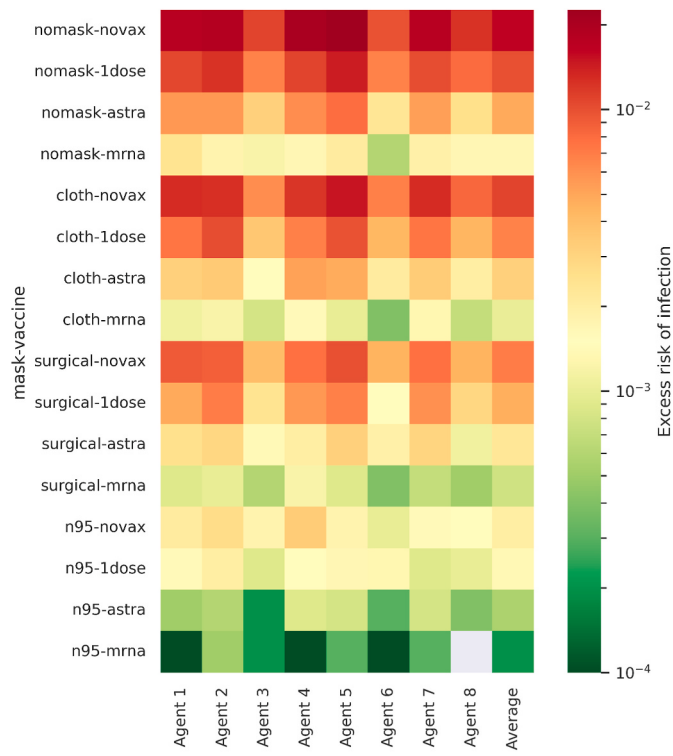


Fig. 8. Average excess risk (probability of infection) experienced per agent from 10,000 simulation runs. Each row in the heatmap denotes one of 16 unique scenario configurations. Each cell shows the final excess risk value reported per agent at the end of the simulation, representing the expected risk experienced through the simulation run-time. Scenario run-time of 210 h was used.

and many challenges in adapting them to new applications.

Our approach places configurability as one of the core tenets, allowing non-experts to deploy the model in many possible environments with reduced integration overhead. With the goal of widespread deployment, high adoptability and ease of integration is necessary in order to maximize the risk-mitigation benefits provided by such software. The agent-based model explored in this paper provides a proof of concept for the technique as applied to our research lab. From our results, it is shown that a wide range of analyses can be performed on the outputs of the model. These analyses provide useful insights for risk mitigation at the policy level for facility administration, as well as a more robust understanding of the consequences of various actions. One such example is the unequally distributed risk of infection across the agents in our lab scenario. Based on the spatial location of agents and their proximity to both other agents and common walking trajectories, their assumed excess risk of infection varies. We observe the logical result of agents in high-traffic areas bearing higher risks of infection, however our model quantifies this risk to provide actionable insights to manage occupant capacity and spatial organization such as seating arrangements. This is particularly important for scenarios with high occupancy limits such as lecture theaters, or scenarios where agents require different levels of risk management, such as immunocompromised individuals in hospitals or LTCFs.

Beyond configurability for different environments, our framework provides the ability to simulate arbitrary epidemiological profiles for diseases beyond COVID-19. This extensibility offers utility beyond modeling COVID-19 outbreaks and can be used for epidemic and pandemic preparedness in the future.

Analyses which compare different simulation scenarios prove useful for evaluating the effectiveness of various policy implementations in the context of specific environments. This utility is demonstrated by the

generated heatmap of average final excess risk in Fig. 8, which can be re-contextualized to relative excess risk by comparing to the population IPR of 0.021. In this context the agent-average result for nomask-novax of 0.015 represents a 75% increased risk of infection which is two orders of magnitude larger than the <1% increased risk associated with n94-mRNA. These results and their corresponding information illustrated in Figs. 4, 5 and 8 will appear as part of a decision support interface, and insights such as these can guide policy to improve public health and reduce clinical resource strain.

6. Conclusions and future work

Our study highlights the utility and insights provided by localized agent-based modeling techniques, as well as the importance of configurability for widespread adoption. Offering a highly configurable and localized agent-based model to facility administrators for assisting in decision support can greatly improve the quality and effects of epidemic and pandemic response, without requiring the explicit input of epidemiologists and other domain experts. Our results demonstrate the style of analysis and insights possible with this proof of concept and offer a strong foundation for future exploration and development.

This study offers three broad avenues for future development: the application and validation of our technique on real-world LTCF data; the development of a formal machine reasoning driven decision support system; and the explicit development of various disease profiles for further simulation. Validating our proof of concept is the next critical step towards eventual adoption and deployment of the technology for real-world applications and environments. Our work with the Brenda Strafford Foundation will potentially see their LTCFs used as a pilot deployment for our framework. Development of a decision support layer above the simulation outputs is also necessary for real-world use. The use of machine reasoning for this decision support system will provide a higher level of interpretability and transparency over conventional machine learning techniques. Lastly, developing additional disease profiles which are available as part of the core framework will be very useful to facilities such as LTCFs where disease outbreaks pose a high risk to the patient cohort and the cost of improper epidemic management is very high.

CRediT authorship contribution statement

P. Ciunkiewicz: Software, Methodology, Results, Study Design, Writing - Original draft preparation. **W. Brooke:** Data Collection, Writing - Original draft preparation. **M. Rogers:** Data Collection. **S. Yanushkevich:** Project Conceptualization, Study Design, Results.

Data availability

Simulation data and code is available upon request from the authors.

Declaration of competing interest

There are no competing interests to declare.

References

- [1] M. Ciotti, M. Ciccozzi, A. Terrinoni, W.-C. Jiang, C.-B. Wang, S. Bernardini, The COVID-19 pandemic, *Crit. Rev. Clin. Lab. Sci.* 57 (2020) 365–388.
- [2] World Health Organization, WHO Coronavirus (COVID-19) Dashboard, 2021. <http://covid19.who.int>.
- [3] C.R. MacIntyre, A.A. Chughtai, A rapid systematic review of the efficacy of face masks and respirators against coronaviruses and other respiratory transmissible viruses for the community, healthcare workers and sick patients, *Int. J. Nurs. Stud.* 108 (2020), 103629.
- [4] H. Ueki, Y. Furusawa, K. Iwatsuki-Horimoto, M. Imai, H. Kabata, H. Nishimura, Y. Kawaoka, Effectiveness of face masks in preventing airborne transmission of SARS-CoV-2, *mSphere* 5 (2020) e00637–20.
- [5] D.K. Chu, E.A. Akl, S. Duda, K. Solo, S. Yaacoub, H.J. Schünemann, D.K. Chu, E. A. Akl, A. El-harakeh, A. Bognanni, T. Lotfi, M. Loeb, A. Hajizadeh, A. Bak, A. Izcovich, C.A. Cuello-Garcia, C. Chen, D.J. Harris, E. Borowiack, F. Chamseddine, F. Schünemann, G.P. Morgan, G.E.U.M. Schünemann, G. Chen, H. Zhao, I. Neumann, J. Chan, J. Khabsa, L. Hneiny, L. Harrison, M. Smith, N. Rizk, P.G. Rossi, P. AbiHanna, R. El-khoury, R. Stalteri, T. Baldeh, T. Piggott, Y. Zhang, Z. Saad, A. Khamis, M. Reinap, S. Duda, K. Solo, S. Yaacoub, H.J. Schünemann, Physical distancing, face masks, and eye protection to prevent person-to-person transmission of SARS-CoV-2 and COVID-19: a systematic review and meta-analysis, *Lancet* 395 (2020) 1973–1987.
- [6] J. Lopez Bernal, N. Andrews, C. Gower, E. Gallagher, R. Simmons, S. Thelwall, J. Stowe, E. Tessier, N. Groves, G. Dabrera, R. Myers, C.N. Campbell, G. Amirthalingam, M. Edmunds, M. Zambon, K.E. Brown, S. Hopkins, M. Chand, M. Ramsay, Effectiveness of Covid-19 vaccines against the B.1.617.2 (delta) variant, *N. Engl. J. Med.* 385 (2021) 585–594.
- [7] N. Ferguson, D. Laydon, G. Nedjati Gilani, N. Imai, K. Ainslie, M. Baguelin, S. Bhatia, A. Boonyasiri, Z. Cucunubá Perez, G. Cuomo-Dannenburg, A. Dighe, I. Dorigatti, H. Fu, K. Gaythorpe, W. Green, A. Hamlet, W. Hinsley, L. Okell, S. Van Elsland, H. Thompson, R. Verity, E. Volz, H. Wang, Y. Wang, P. Walker, P. Winskill, C. Whittaker, C. Donnelly, S. Riley, A. Ghani, Report 9: Impact of Non-pharmaceutical Interventions (NPIs) to Reduce COVID19 Mortality and Healthcare Demand, Imperial College London, 2020. Technical Report, <http://spiral.imperial.ac.uk/handle/10044/1/77482>.
- [8] E. Bonabeau, Agent-based modeling: methods and techniques for simulating human systems, *Proc. Natl. Acad. Sci. Unit. States Am.* 99 (2002) 7280–7287.
- [9] C. Macal, M. North, Introductory tutorial: agent-based modeling and simulation, in: Proceedings of the Winter Simulation Conference 2014, 2014, pp. 6–20, <https://doi.org/10.1109/WSC.2014.7019874>.
- [10] E. Cuevas, An agent-based model to evaluate the COVID-19 transmission risks in facilities, *Comput. Biol. Med.* 121 (2020), 103827.
- [11] M.R. Bicher, C. Rippinger, C. Urach, D. Brunmeir, N. Popper, Evaluation of Contact-Tracing Policies against the Spread of SARS-CoV-2 in Austria: An Agent-Based Simulation, *Medical Decision Making* 41 (2021) 1017–1032, <https://doi.org/10.1177/0272989X211013306>.
- [12] L.K.N. Nguyen, S. Howick, D. McLafferty, G.H. Anderson, S.J. Pravinkumar, R.V. D. Meer, I. Megiddo, Evaluating intervention strategies in controlling coronavirus disease 2019 (COVID-19) spread in care homes: an agent-based model, *Infect. Control Hosp. Epidemiol.* (2020) 1–11.
- [13] M. D’Orazio, G. Bernardini, E. Quagliarini, How to restart? An agent-based simulation model towards the definition of strategies for COVID-19 “second phase” in public buildings, *arXiv* (2020).
- [14] S.L. Chang, N. Harding, C. Zachreson, O.M. Cliff, M. Prokopenko, Modelling transmission and control of the COVID-19 pandemic in Australia, *Nat. Commun.* 11 (2020) 5710.
- [15] T.N. Vilches, S. Nourbakhsh, K. Zhang, L. Juden-Kelly, L.E. Cipriano, J.M. Langley, P. Sah, A.P. Galvani, S.M. Moghadas, Multifaceted strategies for the control of COVID-19 outbreaks in long-term care facilities in Ontario, Canada, *Prev. Med.* 148 (2021), 106564.
- [16] R.J. Rockett, A. Arnott, C. Lam, R. Sadsad, V. Timms, K.-A. Gray, J.-S. Eden, S. Chang, M. Gall, J. Draper, E.M. Sim, N.L. Bachmann, I. Carter, K. Basile, R. Byun, M.V. O’Sullivan, S.C.-A. Chen, S. Maddocks, T.C. Sorrell, D.E. Dwyer, E.C. Holmes, J. Kok, M. Prokopenko, V. Sintchenko, Revealing COVID-19 transmission in Australia by SARS-CoV-2 genome sequencing and agent-based modeling, *Nat. Med.* 26 (2020) 1398–1404.
- [17] N. Mahdizadeh Gharakhanlou, N. Hooshangi, Spatio-temporal simulation of the novel coronavirus (COVID-19) outbreak using the agent-based modeling approach (case study: Urmia, Iran), *Inform. Med. Unlocked* 20 (2020), 100403.
- [18] P. Kumar, V.S. Erturk, M. Murillo-Arcila, A new fractional mathematical modelling of COVID-19 with the availability of vaccine, *Results Phys.* 24 (2021), 104213.
- [19] P. Kumar, V.S. Erturk, M. Murillo-Arcila, R. Banerjee, A. Manickam, A case study of 2019-nCoV cases in Argentina with the real data based on daily cases from March 03, 2020 to March 29, 2021 using classical and fractional derivatives, *Adv. Differ. Equ.* 2021 (2021) 341.
- [20] P. Kumar, V.S. Erturk, K.S. Nisar, W. Jamshed, M.S. Mohamed, Fractional dynamics of 2019-nCoV in Spain at different transmission rate with an idea of optimal control problem formulation, *Alex. Eng. J.* 61 (2022) 2204–2219.
- [21] D. Adam, Special report: the simulations driving the world’s response to COVID-19, *Nature* 580 (2020) 316–318.
- [22] Centers for Disease Control and Prevention, Principles of Epidemiology in Public Health Practice, third ed., 2020. <https://www.cdc.gov/csels/dsepd/ss1978/glossary.html>.
- [23] V. Vuorinen, M. Aarnio, M. Alava, V. Alopaeus, N. Atanasova, M. Auvinen, N. Laabu, N. Subramanian, H. Bordbar, P. Erästö, R. Grande, N. Hayward, A. Hellsten, S. Hostikka, J. Hokkanen, O. Kaario, A. Karvinen, I. Kivistö, M. Korhonen, R. Kosonen, J. Kuusela, S. Lestinen, E. Laurila, H.J. Nieminen, P. Peltonen, J. Pokki, A. Puisto, P. Räbäck, H. Salmenjoki, T. Sironen, M. Österberg, Modelling aerosol transport and virus exposure with numerical simulations in relation to SARS-CoV-2 transmission by inhalation indoors, *Saf. Sci.* 130 (2020), 104866.
- [24] C. McAloon, A. Collins, K. Hunt, A. Barber, A.W. Byrne, F. Butler, M. Casey, J. Griffin, E. Lane, D. McEvoy, P. Wall, M. Green, L. O’Grady, S.J. More, Incubation period of COVID-19: a rapid systematic review and meta-analysis of observational research, *BMJ Open* 10 (2020), e039652.
- [25] A.W. Byrne, D. McEvoy, A.B. Collins, K. Hunt, M. Casey, A. Barber, F. Butler, J. Griffin, E.A. Lane, C. McAloon, K. O’Brien, P. Wall, K.A. Walsh, S.J. More, Inferred duration of infectious period of SARS-CoV-2: rapid scoping review and analysis of available evidence for asymptomatic and symptomatic COVID-19 cases, *BMJ Open* 10 (2020), e039856.

- [26] The Lancet Respiratory Medicine, COVID-19 transmission—up in the air, the Lancet, Respir. Med. 8 (2020) 1159.
- [27] E.L. Anderson, P. Turnham, J.R. Griffin, C.C. Clarke, Consideration of the aerosol transmission for COVID-19 and public health, Risk Anal. 40 (2020) 902–907.
- [28] N. van Doremalen, T. Bushmaker, D.H. Morris, M.G. Holbrook, A. Gamble, B. N. Williamson, A. Tamin, J.L. Harcourt, N.J. Thornburg, S.I. Gerber, J.O. Lloyd-Smith, E. de Wit, V.J. Munster, Aerosol and surface stability of SARS-CoV-2 as compared with SARS-CoV-1, N. Engl. J. Med. 382 (2020) 1564–1567.
- [29] Government of Canada, COVID-19 Daily Epidemiology Update, last Modified: 2021-04-08, 2020, <https://health-infobase.canada.ca/covid-19/epidemiological-summary-covid-19-cases.html>.
- [30] O. Byambasuren, M. Cardona, K. Bell, J. Clark, M.-L. McLaws, P. Glasziou, Estimating the extent of asymptomatic COVID-19 and its potential for community transmission: systematic review and meta-analysis, Off. J. Assoc. Med. Microbiol. Infect. Dis. Canada 5 (4) (2020) 223–234, <https://doi.org/10.3138/jammi-2020-0030>.
- [31] W.O. Kermack, A.G. McKendrick, A contribution to the mathematical theory of epidemics, Proc. R. Soc. Lond. - Ser. A Contain. Pap. a Math. Phys. Character 115 (1927) 700–721.
- [32] Public Health Agency of Canada, COVID-19: How to Quarantine (Self-isolate) at Home when You May Have Been Exposed and Have No Symptoms, 2020. <https://www.canada.ca/en/public-health/services/publications/diseases-conditions/coronavirus-disease-covid-19-how-to-self-isolate-home-exposed-no-symptoms.html>.
- [33] P.E. Hart, N.J. Nilsson, B. Raphael, A formal basis for the heuristic determination of minimum cost paths, IEEE Trans. Syst. Sci. Cybern. 4 (1968) 100–107.
- [34] X. Liu, D. Gong, A comparative study of A-star algorithms for search and rescue in perfect maze, in: 2011 International Conference on Electric Information and Control Engineering, 2011, pp. 24–27, <https://doi.org/10.1109/ICEICE.2011.5777723>.